Supplementary Materials

Hydrothermal Sintering and Oxidation of an Alumina-Supported Nickel Methanation Catalyst Studied using *in situ* Magnetometry

Malebelo Maphutha, Dominic de Oliveira, Thulani M. Nyathi, Mohamed I. Fadlalla, Robert Henkel, Nico Fischer, Michael Claeys*

*Catalysis Institute and c*change (DSI-NRF Centre of Excellence in Catalysis), Department of Chemical Engineering, University of Cape Town, Rondebosch 7701, South Africa*

Powder X-ray diffraction

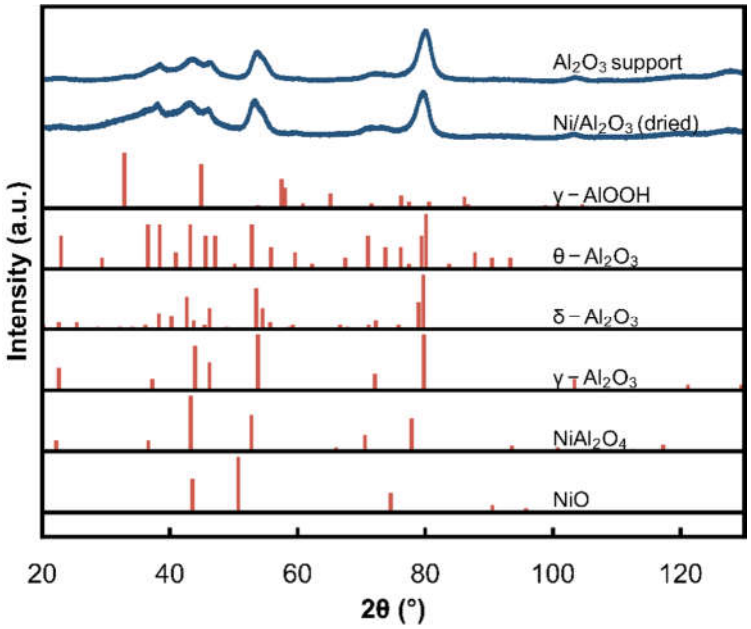

Figure S1: *Ex situ* PXRD pattern of the bare and Ni-loaded Al_2O_3 support (radiation source: Co Kα1 = 1.78897 Å). Also included are the reference reflection lines of NiO, $NiAl_2O_4$, γ-Al_2O_3, δ-Al_2O_3, θ-Al_2O_3 and γ-AlOOH obtainned from the ICDD PDF-2 database [2] – also see PDF-2 entries in Table S1. The Al-containing crystal phases considered are those reported by the manufacturer to be present in the Al_2O_3 support [3].

Table S.1: ICDD PDF-2 entries of all chemical/crystal phases relevant to the current study.

Chemical formula	Chemical name	Entry
γ-AlOOH	γ-Aluminium oxyhydroxide	01-072-0359

γ-Al_2O_3	γ-Aluminium oxide	00-010-0425
δ-Al_2O_3*	δ-Aluminium oxide	00-016-0394
θ-Al_2O_3	θ-Aluminium oxide	00-011-0517
$NiAl_2O_4$	Nickel(II) aluminate or nickel(II) aluminium oxide	00-010-0339
NiO	Nickel(II) oxide	00-047-1049

* full crystallographic information not available in the ICDD PDF-2 database.

Transmission electron microscopy (TEM)

$$number-based\ average\ (\bar{d}_{c,n}) = \frac{\sum_{i=1}^{N} n_i d_i}{N} \quad \text{(S1)}$$

$$volume-based\ average\ (\bar{d}_{c,v}) = \frac{\sum_{i=1}^{N} n_i d_i^4}{\sum_{i=1}^{N} n_i d_i^3} \quad \text{(S2)}$$

$$number-based\ standard\ deviation\ (sd_n) = \sqrt{\frac{\sum_{i=1}^{N} n_i \left(d_i - \bar{d}_{c,n}\right)^2}{N-1}} \quad \text{(S3)}$$

$$volume-based\ standard\ deviation\ (sd_v) = \sqrt{\frac{\sum_{i=1}^{N} n_i d_i^3 \left(d_i - \bar{d}_{c,v}\right)^2}{\frac{N-1}{N}\sum_{i=1}^{N} n_i d_i^3}} \quad \text{(S4)}$$

d_i is the diameter of particle i, n_i is the number of particles of size d_i and N is the total number of particles counted. The above equations can also be found in the book chapter by Bergeret and Gallezot [1].

Magnetometer calibration

100 mg of bulk nickel oxide was placed into the *in situ* magnetometer. The sample was then heated to 700 °C (heating rate: 4 °C/min) in 100 mL (NTP)/min of hydrogen. Thereafter, the gas was changed from hydrogen to argon (100 mL (NTP)/min) and held for 2 hours. The sample was then cooled to 25 °C (cooling rate: 1 °C/min) and held at 25 °C for 3 hours. A calibration factor was obtained for the *in situ* magnetometer by comparing the mass specific saturation magnetisation of Ni at 27 °C, reported as 43.8 emu/g (Gong, *et al*., 1991), with the signal obtained in the *in situ* magnetometer for a known mass of Ni at the same temperature (3.13 a.u./g). Multiplying the two together results in a calibration factor for the *in situ* magnetometer – 14 emu/a.u. This converts the signal to magnetic units.

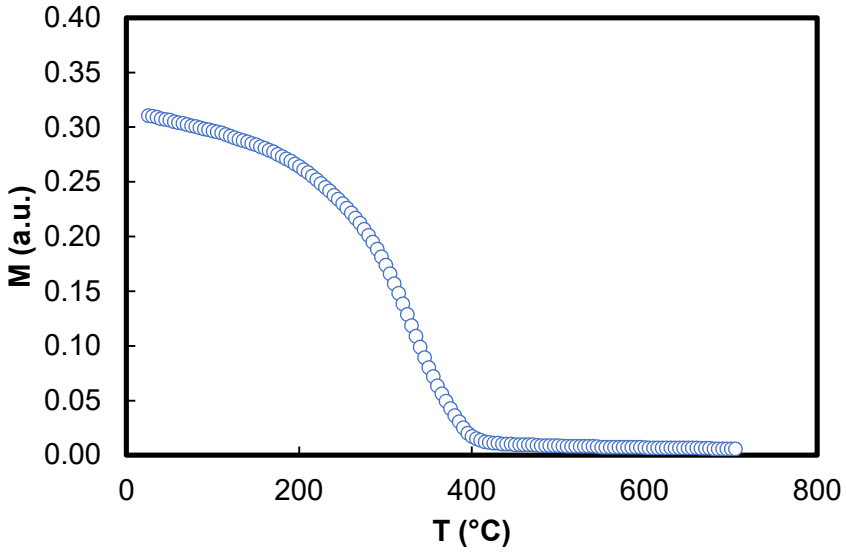

Figure S2: Calibration curve for the magnetometer based on 0.1 g of unreduced and unsupported NiO.

Thermodynamics

The thermodynamic stability of Ni toward the formation of NiO and $NiAl_2O_4$ has been studied, with the P_{H_2O}/P_{H_2} required to oxidise Ni^0 as a function of temperature presented in Figure S2. The equilibrium position was calculated based on the reactions in Equations S5 and S6, with the required thermodynamic data being obtained from Knacke, Kubaschewski and Hesselmann [1].

$$Ni + H_2O \rightarrow NiO + H_2 \quad \text{S5}$$

$$Ni + Al_2O_3 + H_2O \rightarrow NiAl_2O_4 + H_2 \quad \text{S6}$$

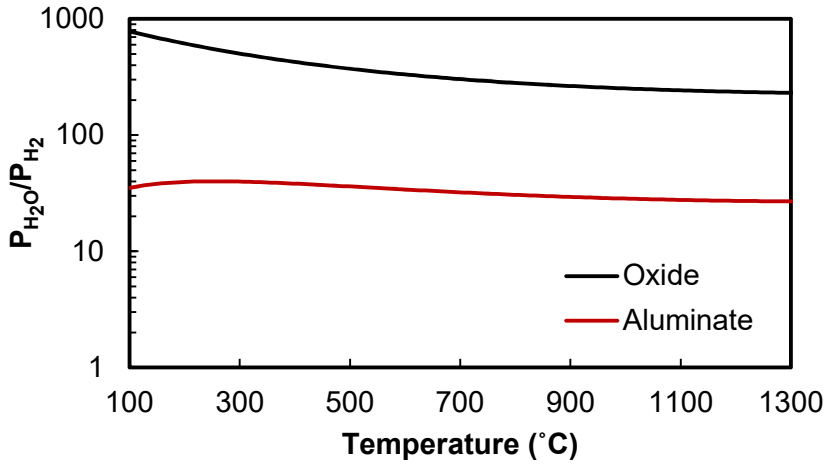

Figure S3: Thermodynamics of the oxidation of metallic Ni to NiO and $NiAl_2O_4$ showing the partial pressure ratio of steam to hydrogen equilibrium position as a function of temperature.

Langevin method results

The evaluation of the Langevin equation at different sizes to demonstrate the effect of particle size on the M-H measurement is shown in Figure S4.

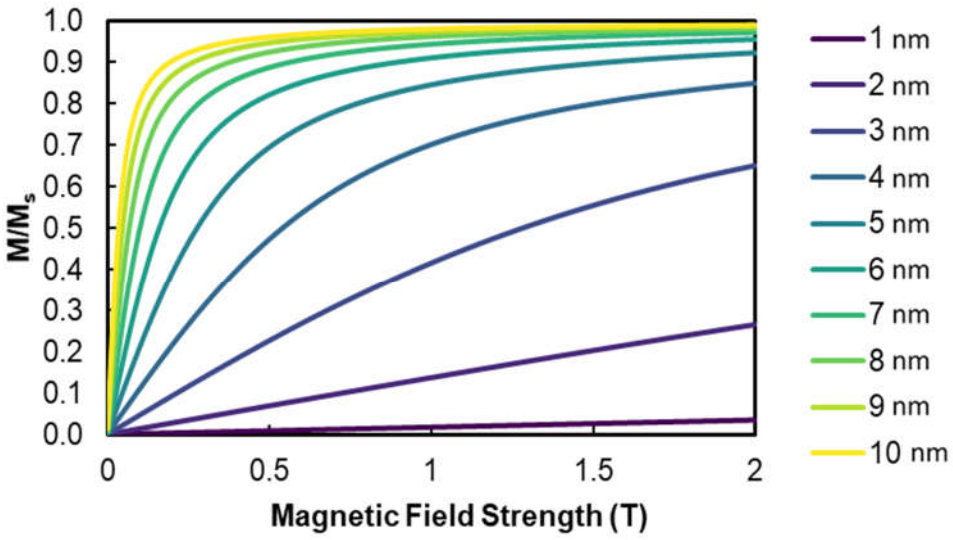

Figure S4: Langevin equation evaluated at sizes ranging from 1 nm to 10 nm.

In order to identify the size distribution which best fits the experimental results, three methods were used. The lognormal fit was carried out generating multiple lognormal distributions with a known mean size and variance, then identifying the distribution with the best fit to the experimental results. The mean of the tested lognormal distributions was varied between 1 and 20 nm, and the variance was varied between 1 and 30 nm. A similar approach was followed for the bimodal fit, where the mean and variance was varied in the same range, however the generated distribution was made up of two lognormal distributions, with both lognormal components being varied. The third method used was a least squares approach, where the sum of squares of the residuals between the Langevin linear combination curve (Equation 5) and the experimental results was minimized. The distributions determined by these three methods for the measurements taken under H_2O environment have been compared and presented in Figure S5. Since the least squares method produced the lowest residual sum of squares, this method was used for all size distributions presented in the results section. The calculated Langevin curves resulting from these distributions have been compared in Figure S6 and Figure S7.

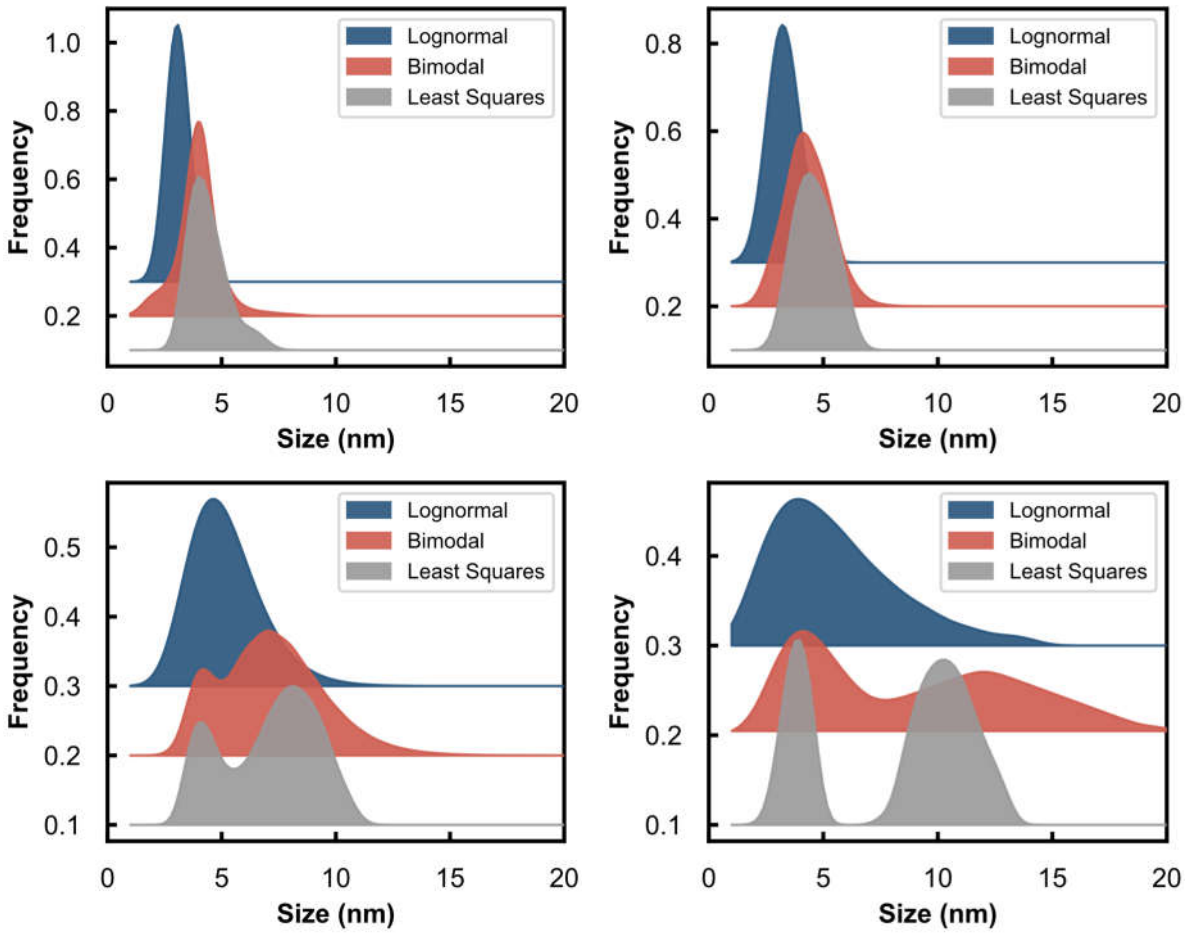

Figure S5: Comparison of size distributions determined by lognormal, bimodal and least squares methods for Langevin analysis of measurements taken under H_2O environment at a) 350 °C, b) 450 °C, c) 550 °C and d) 650 °C.

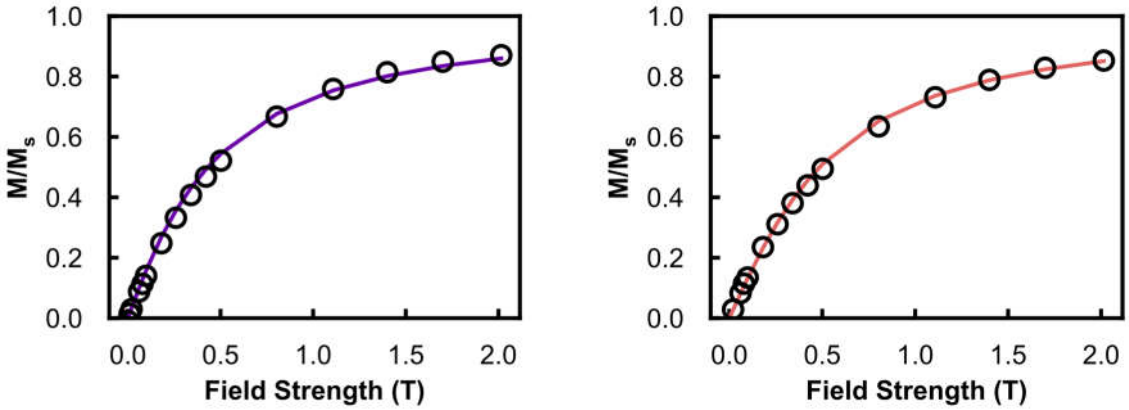

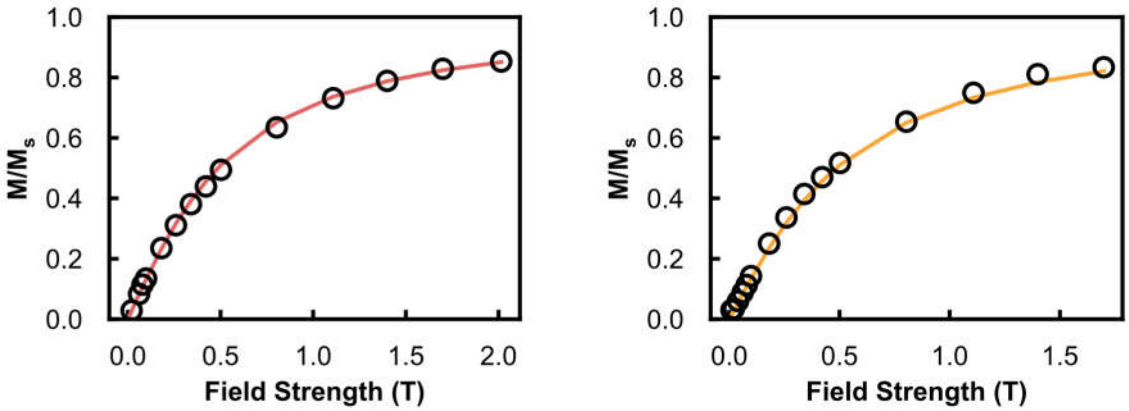

Figure S6: Calculated (-) and experimentally measured (o) Langevin curves for catalyst tested in Ar environment at a) 350 °C, b) 450 °C, c) 550 °C and d) 650 °C.

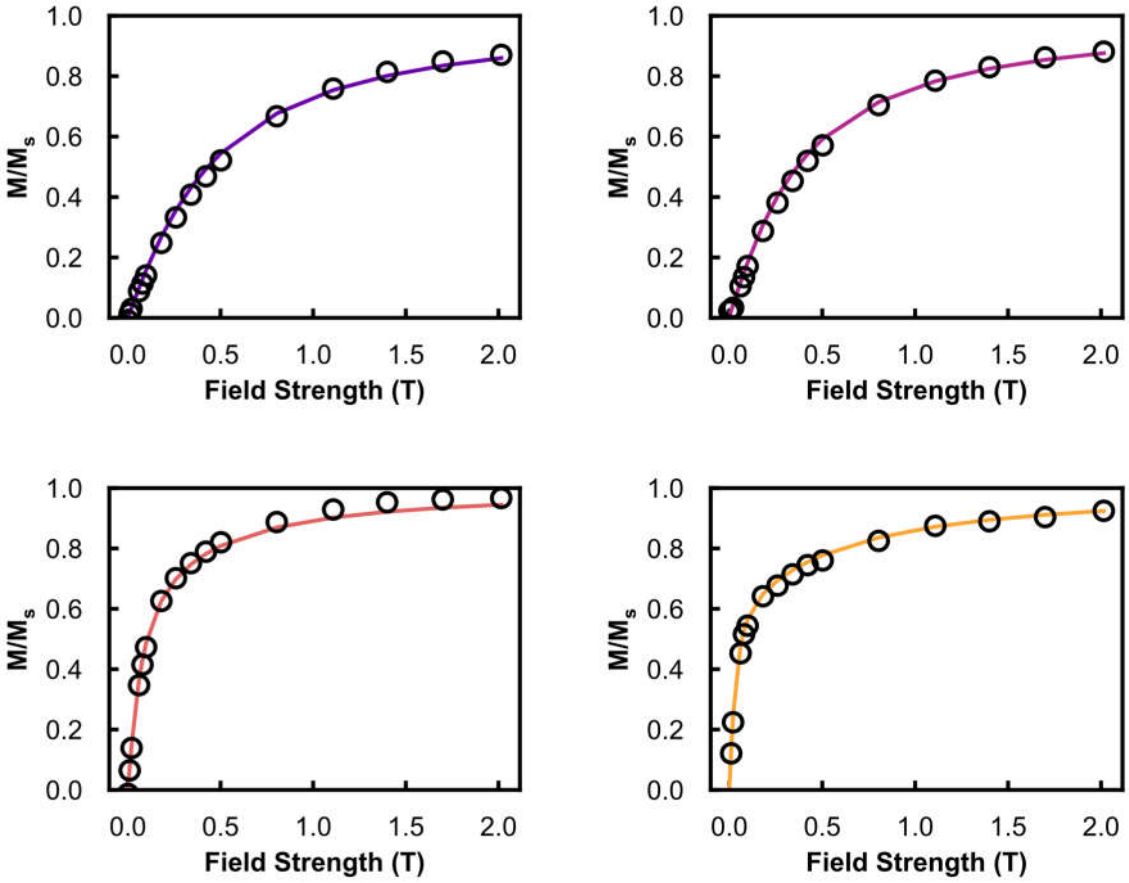

Figure S7: Calculated (-) and experimentally measured (o) Langevin curves for catalyst tested in H_2O environment at a) 350 °C, b) 450 °C, c) 550 °C and d) 650 °C.

Comparison between magnetometry-based and TEM size distributions

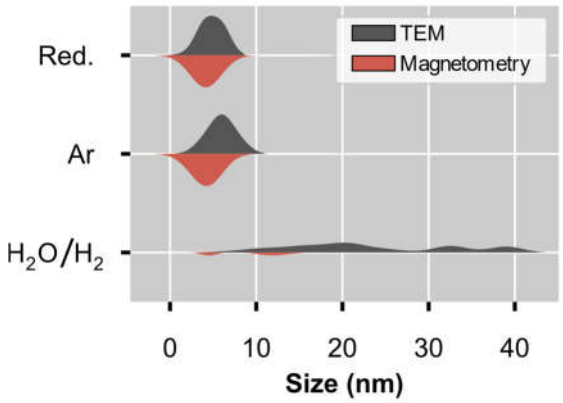

Figure S8: Comparison of the volume-based size distributions derived using the data from *ex situ* TEM and *in situ* magnetometry, with the size distributions normalised to their respective areas.

References

1. Bergeret, G.; Gallezot, P. Particle Size and Dispersion Measurements. In *Handbook of Heterogeneous Catalysis*; Ertl, G., Knözinger, H., Schüth, F., Weitkamp, J., Eds.; Wiley-VCH Verlag GmbH & Co. KGaA: Weinheim, Germany, 2008; pp. 738–765.
2. ICDD PDF-2 Release 2008 (Database), International Centre for Diffraction Data, Newtown Square, PA, USA, 2008.
3. SASOL PURALOX and CATALOX, https://products.sasol.com/pic/products/home/grades/AS/5puralox-and-catalox/index.html (accessed February 2020).
4. Knacke, O. Kubaschewski, K. Hesselmann, Thermochemical properties of inorganic substances, 2nd ed ed., Springer-Verlag, Berlin, 1991.